CIRP Annals - Manufacturing Technology 66 (2017) 217–220

Contents lists available at ScienceDirect

CIRP Annals - Manufacturing Technology

journal homepage: http://ees.elsevier.com/cirp/default.asp

Evaluation of energy density measures and validation for powder bed fusion of polyamide

David Bourell (2)[a,*], Jeremiah Coholich [a], Antoine Chalancon [b], Abhimanyu Bhat [a]

[a] Laboratory for Freeform Fabrication, Mechanical Engineering Department, The University of Texas at Austin, Austin, Texas, USA
[b] Department of Mechanical Engineering, ENISE, Saint-Étienne, France

ARTICLE INFO

Article history:
Available online 2 May 2017

Keywords:
Polymer
Measurement
Additive manufacturing

ABSTRACT

For powder bed fusion additive manufacturing, energy density captures the interrelated effects of beam power/size, scanning speed, hatch spacing and layer thickness. Relations for energy density include linear, areal and volumetric forms, developed empirically or theoretically. Various energy density formulations for laser sintering of polyamide 12 were evaluated based on correlation to measured part mass relative densities. Test pieces were printed with varying parameters: laser power, hatch spacing and layer thickness. Results show that total energy density is correlated to both and mass density and strength for a volumetric energy density.

1. Introduction

1.1. Energy density in additive manufacturing

The properties and structure of polymer parts created using powder-bed fusion additive manufacturing processes are dependent on processing parameters during manufacture. This includes typically parameters such as the energy beam power, beam size, scan speed, layer thickness and spacing between scan tracks ("hatch spacing"). It is helpful to construct a single parameter set that captures the effect of processing parameters on salient part properties including density and mechanical properties. This parameter set historically has taken the form of an energy density ED which in general takes the form:

$$ED = \frac{P}{f(v, D, H, \lambda)} \quad (1)$$

where P = energy beam power, v = scan speed, D = energy beam diameter, H = scan or hatch spacing, the distance between scan tracks, and λ = layer thickness. The energy density has been written as an energy on a linear, areal or volume basis. The areal form is effectively an energy flux, the energy crossing the surface of a powder bed into the feedstock. All forms of energy density equation are based on an assumption that the laser delivers a uniform level of power over the beam diameter. The distribution is actually Gaussian. This may impact correlation with experiment, particularly when the scan spacing is large compared to the laser diameter.

1.2. Energy density forms

1.2.1. Volume energy density

A macroscopic volume-based energy density for additive manufacturing was first derived by Nelson [1] and then advanced by Starr et al. [2,3]. The volume energy density is:

$$ED_{vH} = \frac{P}{vH\lambda} \quad (2)$$

The equation may be derived macroscopically as the total energy imparted to the part during the build divided by the part volume V. Take the total energy to be E = Pt where t is the total scan time. For simplicity, assume a rectangular part is created with xy area A = ab and height c. The time required to scan one layer t_1 = (ab)/Hv, and there are c/λ layers to scan. The total time t = (abc)/(vHλ) = V/(vHλ). The energy E = Pt = PV/(vHλ), and on a volume basis, the energy density becomes ED_v = P/(vHλ).

The energy density on a volume basis may also be derived on a microscopic basis. Per Fig. 1, the energy beam has diameter D.

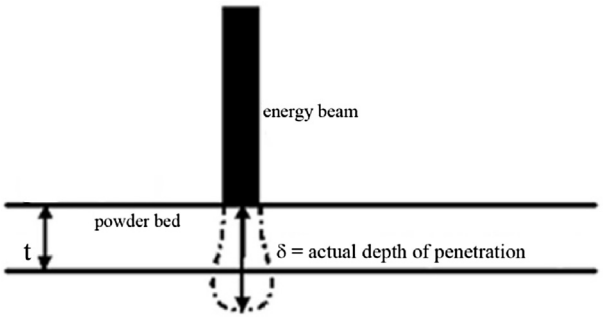

Fig. 1. Powder bed and energy beam penetration.

* Corresponding author at: Laboratory for Freeform Fabrication, Mechanical Engineering Department, The University of Texas at Austin, 204 E. Dean Keeton St., Austin, Texas, USA 78712.

http://dx.doi.org/10.1016/j.cirp.2017.04.128
0007-8506/

There is an illustrated energy interaction volume V_i which may be considered for example to be a melt pool. The energy density may be written as Pt/V_i, where $t = D/v$ and $V_i \approx \pi D^2\delta/4$. Combining and simplifying yields

$$ED_{vD} = \frac{4P}{\pi vD\delta} \approx \frac{P}{vD\delta} \quad (3)$$

Measuring δ experimentally is difficult. As an approximation, the energy interaction distance δ taken to be the layer thickness λ which moves Eq. (3) toward Eq. (2) in form.

1.2.2. Areal energy density

The oldest form of energy density for additive manufacturing is the Andrew Number A, an empirical expression of the energy incident on a surface of the powder bed [1,4]:

$$A_n = \frac{P}{vH} \quad (4)$$

Calculation of the incident energy at a point on an areal basis yields a similar form to Eqs. (3) and (4) [5–8]:

$$ED_A = \frac{P}{vD} \quad (5)$$

Eqs. (4) and (5) show similarities to Eqs. (2) and (3), respectively, with the length dimension (λ or δ) removed. Since there is no depth term, the areal forms do not involve any assumptions of the interaction volume morphology.

1.2.3. Linear energy density

Gu, et al. [9,10] proposed a linear energy density, obtained effectively by removing the length dimension (H or D) from Eqs. (4) and (5):

$$ED_L = \frac{P}{v} \quad (6)$$

2. Experimental

Polyamide 12 cubes of side dimension 25.4 mm were printed using laser sintering. Feedstock ALM PA650 was obtained from Advanced Laser Materials, Temple TX, USA. A DTM Vanguard Sinterstation™ with the HiQ upgrade was used to construct the cubes. The chamber was heated to 173 °C in a nitrogen atmosphere. Scan speed and laser beam diameter were kept constant at 10.2 m/s and 0.5 mm, respectively. The build was divided into three groups of 20 parts each of 75, 100, and 125 μm layer thickness. Within each of these groups, there were two series with 10 parts each. In one series, the scan spacing was kept constant at 250 μm while the laser power was set initially at 10 W and increased by 5 W increments to 55 W. In the second series, the laser power was held constant for all parts at 24 W while the scan spacing was increased by 25 μm increments from 75 μm to 300 μm.

The energy densities for each part were calculated using the printing parameters and Eqs. (2)–(6). Density was determined using a mensuration technique based on mass and cube dimension measurement using a Vernier caliper. Mass was measured using a Denver Instruments APX-200 balance with 0.1 mg resolution. The Vernier caliper resolution was 0.01 mm. Multiple measurements were taken and averaged.

Tensile specimens were prepared in accordance with the ASTM D638 standard for tension testing of plastics. These specimens were divided into three groups of 75, 100, and 125 μm layer thickness. Each group of tensile specimens at a constant layer thickness was further divided into three subgroups with scan spacing of 100, 200, and 300 μm. In each of these subgroups, laser power was varied from 10 W to 45 W, with increments of 5 W. The tensile specimens were tested using an Instron® 3300 series mechanical testing station. The tensile strength of each of the specimens was recorded, and plotted with respect to the volumetric energy density calculated using Eq. (2).

3. Results

Fig. 2 shows the results as the effect of part density on the form of the energy density relationship. The left column of Fig. 2 shows varying layer thickness effects, and the right column shows hatch/scan spacing effects. The plots show effects of varying laser power, layer thickness and hatch spacing on part density. Considering the left column of varying laser power and layer thickness, results show a monotonic relationship of energy density to part density for the volume energy density formulations (Eqs. (2) and (3)). Areal and linear energy density formulations capture accurately the trend of increasing part density with energy density, but there is a divergence of the curves based on layer thickness values. For the right column of varying hatch spacing and layer thickness, it is seen that the energy density formulations based on Eqs. (3), (5) and (6) do not generate a monotonic relationship. This is a result of the lack of inclusion of hatch spacing as a parameter in the formulation, while experimentally the hatch spacing clearly affects the part density. The Andrew Number, the empirical areal formulation of energy density based on Eq. (4) illustrated in Fig. 2c, shows scatter based on a lack of inclusion of layer thickness in its formulation.

Figs. 3 and 4 were plotted to summarize the effect of macroscopic volume energy density on the final part density and tensile strength. These plots indicate that both density and tensile strength show a rapid improvement with increase in energy density initially, and then a small improvement as these properties reach a maximum value.

4. Discussion

To be an effective processing parameter, the energy density indicator should exhibit a one-to-one correspondence with an output metric, typically mass density and/or mechanical properties. In general, the laser power is the key variable altered when investigating machine parameter effects on laser sintering part quality, with scan speed, layer thickness, hatch spacing and beam size all held constant. Under these circumstances, all energy density formulations provide a reasonable monotonic form, at least as related to mass density of the part. However, as illustrated in Fig. 2, only the macroscopic volume-based energy density expressed in Eq. (2) accurately incorporates the effects of varying layer thickness and hatch spacing.

The models for energy density based on an isolated energy beam scanning an undisturbed powder bed, Eqs. (3), (5) and (6), fundamentally do not consider the hatch spacing. For actual laser sintering, the hatch spacing affects the part quality and should be included. The Andrew Number does not include the layer thickness which is shown to impact part quality as well.

Based on these results, the model for energy density for laser sintering that best incorporates the effects of the stated process parameters is the macroscopic volume energy density based on a calculation of total energy input to the part normalized by the part volume, Eq. (2). Fig. 3 shows a compilation plot of this formulation for all data in this investigation. This volume energy density formulation is seen to reasonably incorporate the effects of laser power, layer thickness and hatch spacing on the mass density. Mass density increases rapidly as a function of energy density up to about 0.12 J/mm^3. The mass density then slowly increases up to an energy density of 0.4 J/mm^3. As observed earlier [2,11], this is consistent with the three-mechanisms of densification for laser sintering. At low energy density, part quality increases with increasing energy density. This is a region for which there is insufficient energy deposition for full densification. The second region shows nominally full mass density and strength with increasing energy density. Here the increasing energy deposition serves primarily to densify the layer and to increase the internal energy of the material. At even higher energy densities, the mass density and strength are shown to decrease with increasing energy density. This is typically associated with material degradation effects which induce porosity [12]. Fig. 4 shows the effect of

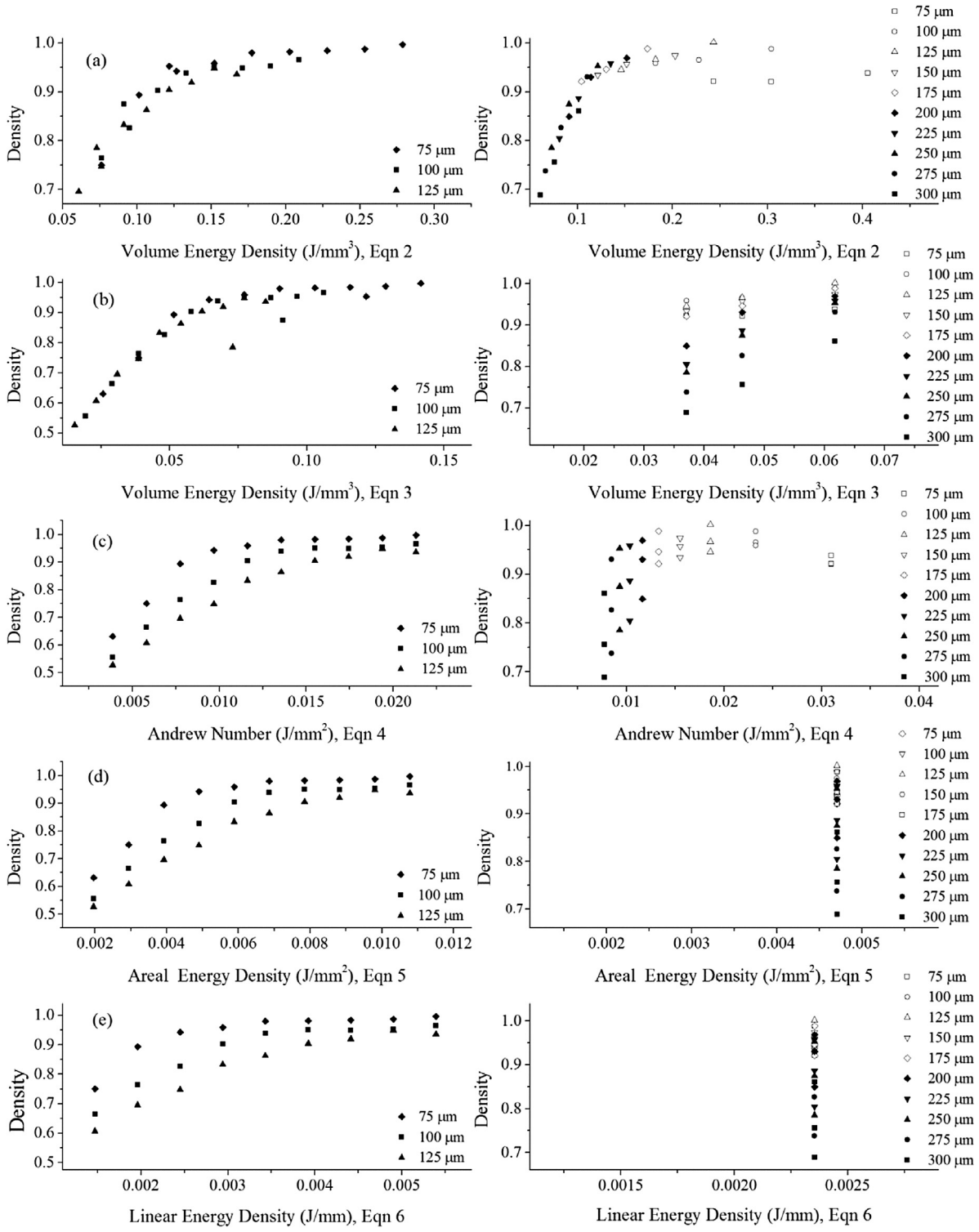

Fig. 2. Effect of layer thickness (left) and hatch/scan spacing (right) on the density of PA-12 laser sintered parts. Energy density for (a)–(e) was calculated based on the formulations in Eqs. (2)–(6), respectively. For the left column, the hatch spacing was constant at 250 µm, and laser powder varied between 10–55 W. For the right column, the laser power was constant at 24 W, and the layer thickness was varied between 75–125 µm.

macroscopic volume energy density (using Eq. (2)) on tensile strength of the laser sintered PA 12 parts. The tensile strength plot follows a similar trend to the mass density, and the tensile strength increases linearly when the macroscopic volumetric energy density is increased up to ~0.12 J/mm^3, and gradually increases as the volume energy density is further increased.

In Fig. 4, it is seen that the tensile strength decreases from a maximum of 51 MPa–47 MPa at macroscopic volume energy densities greater than 0.3 J/mm^3. At higher energy densities, the powder surrounding the parts in the part bed fuses with the part during the laser sintering process, a phenomenon termed "part growth" or "Bonus Z" [13,14]. This leads an incompletely fused outer layer on the part surface, which does not contribute significantly to strength but causes an increase in the dimensions used for tensile stress calculations. The decrease in the tensile strength in this study is attributed to the formation of this outer layer. This effect of the incompletely fused outer layer can also be observed in Fig. 3 mass density plot to a lesser extent, since the maximum energy density there was held to 0.4 J/mm^3 rather than 0.6 J/mm^3 for the mechanical property study.

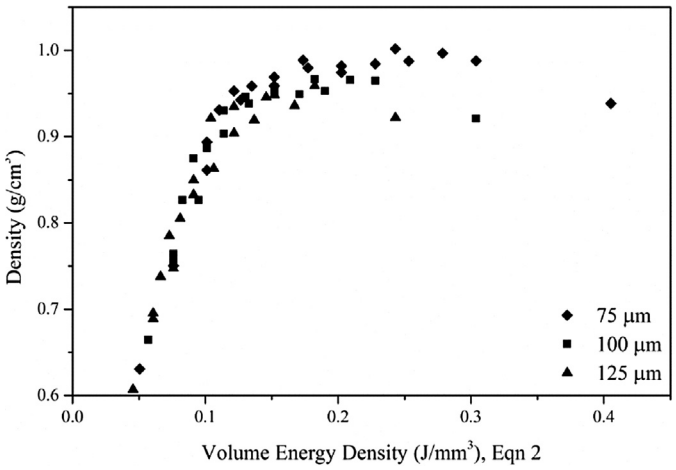

Fig. 3. The effect of volume energy density (Eq. (2)) on mass density of a laser sintered PA-12 part. Results include varying laser power, layer thickness and hatch spacing.

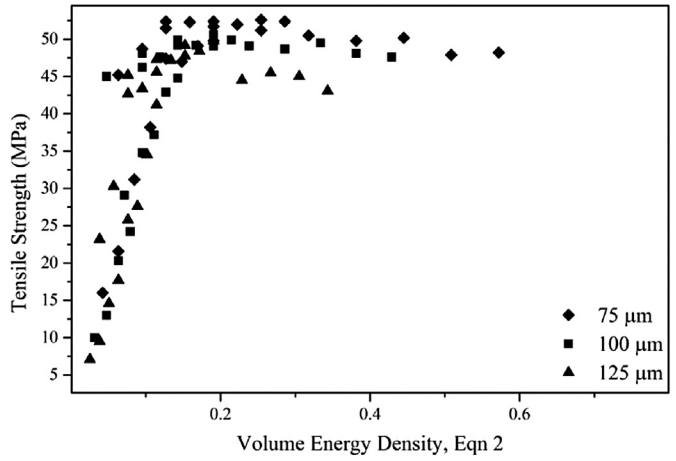

Fig. 4. The effect of volume energy density (Eq. (2)) on tensile strength of a laser sintered PA-12 part. Results include varying laser power, layer thickness and hatch spacing.

5. Summary and Conclusions

Energy density has been used in various forms for many years to capture the effects of various processing parameters on part quality in additive manufacturing powder bed fusion and directed energy deposition processes. Formulations have been proposed based on lineal, areal and volume bases. The objective of this study was to compare the capability of five formulations of energy density to correlate to the resulting mass density and tensile strength for laser sintered polyamide 12. Several formulations fail to incorporate the effect of either layer thickness or hatch spacing, and both are shown to have an effect on mass density and strength.

The formation of energy density that best incorporates all important processing parameters is the macroscopic volume energy density based on a calculation of the total energy deposited into the part on a volume basis, Eq. (1).

Acknowledgments

One of the authors (AC) performed this research while serving as an intern at The University of Texas at Austin under funding from the Department of Mechanical Engineering at the Ecole Nationale d'Ingénieurs de Saint-Etienne, France. The research was partially supported by funding from Structured Polymers, Austin Texas, USA.

References

[1] Nelson JC (1993) *Selective Laser Sintering: A Definition of the Process and an Empirical Sintering Model Doctoral Dissertation*, University of Texas, Austin, TX, USA.
[2] Starr TL, Gornet TJ, Usher JS (2011) The Effect of Process Conditions on Mechanical Properties of Laser-sintered Nylon. *Rapid Prototyping Journal* 17 (6):418–423.
[3] Starr TL, Rafi K, Stucker B, Scherzer CM (2012) Controlling Phase Composition in Selective Laser Melted Stainless Steels. *Proceedings of the Solid Freeform Fabrication Symposium*, Austin, TX, USA, 439–446.
[4] Ho HC, Gibson I, Cheung LW (1999) Effects of Energy Density on Morphology and Properties of Selective Laser Sintered Polycarbonate. *Journal of Materials and Processing Technology* 89:204–210.
[5] Beal VE, Paggi RA, Salmoria GV, Lago A (2009) Statistical Evaluation of Laser Energy Density Effect on Mechanical Properties of Polyamide Parts Manufactured by Selective Laser Sintering. *Journal of Applied Polymer Science* 113 (5):2910–2919.
[6] Caulfield B, McHugh PE, Lohfeld S (2007) Dependence of Mechanical Properties of Polyamide Components on Build Parameters in the SLS Process. *Journal of Materials Processing Technology* 182(1–3):477–488.
[7] Hopkinson N, Majewski CE, Zarringhalam H (2009) Quantifying the Degree of Particle Melt in Selective Laser Sintering. *CIRP Annals – Manufacturing Technology* 58(1):197–200.
[8] Lu L, Fuh J, Wong YS (2001) *Laser-Induced Materials and Processes for Rapid Prototyping*, Springer, US. http://dx.doi.org/10.1007/978-1-4615-1469-5.
[9] Gu D, Wang H, Chang F, Dai D, Yuan P, Hagedorn Y-C, Meiners W (2014) Selective Laser Melting Additive Manufacturing of TiC/AlSi10Mg Bulk-form Nanocomposites with Tailored Microstructures and Properties. *Physics Procedia* 56:108–116.
[10] Gu DD, Shen YF (2009) Effects of Processing Parameters on Consolidation and Microstructure of W–Cu Components by DMLS. *Journal of Alloys and Compounds* 473:107–115.
[11] Tontowi AE, Childs THC (2001) Density Prediction of Crystalline Polymer Sintered Parts at Various Powder Bed Temperatures. *Rapid Prototyping Journal* 7(3):180–184.
[12] Negi S, Sharma Rajesh K (2016) Study on Shrinkage Behaviour of Laser Sintered PA 3200GF Specimens Using RSM and ANN. *Rapid Prototyping Journal* 22 (4):645–659.
[13] Ho H, Gibson I, Cheung W (2000) Effects of Energy Density on Bonus Z, Surface Roughness and Warpage of Selective Laser Sintered Polycarbonate. *The Eighth International Conference on Rapid Prototyping*, Tokyo, Japan, 99–104.
[14] Sercombe TB, Hopkinson N (2006) Process Shrinkage and Accuracy During Indirect Laser Sintering of Aluminium. *Advanced Engineering Materials* 8 (4):260–264.